TYPE Original Research
PUBLISHED 01 October 2025
DOI 10.3389/frlct.2025.1688689



OPEN ACCESS

EDITED BY
Zibusiso Ndlovu,
Médecins Sans Frontières, South Africa

REVIEWED BY
Jerome Rajendran,
University of California, Irvine, United States
Nurul Asmak Md Lazim,
University of Technology Malaysia, Malaysia

*CORRESPONDENCE
Alfredo E. Ongaro,
a.ongaro@onalabs.com

†These authors share first authorship

RECEIVED 19 August 2025
ACCEPTED 11 September 2025
PUBLISHED 01 October 2025

CITATION
Rabost-Garcia G, Sanchez D, Nacher-Castellet V, Fajardo A, Ymbern O, Muñoz-Pascual X, Alvarez A, Punter-Villagrasa J, Casals-Terré J, Heredia R, Espinoza F, Moreno-Simonet L, Cosio PL, Cadefau JA, Marwede M and Ongaro AE (2025) Early-stage life cycle assessment for sustainable design of wearable microfluidic sweat sensor: continuous dehydration monitoring. *Front. Lab Chip Technol.* 4:1688689. doi: 10.3389/frlct.2025.1688689



# Early-stage life cycle assessment for sustainable design of wearable microfluidic sweat sensor: continuous dehydration monitoring

Genis Rabost-Garcia[1,2†], David Sanchez[3†], Victor Nacher-Castellet[1,4,5], Andrea Fajardo[1], Oriol Ymbern[1], Xavier Muñoz-Pascual[1], Albert Alvarez[1], Jaime Punter-Villagrasa[1], Jasmina Casals-Terré[2], Ricardo Heredia[6], Fernando Espinoza[6], Lia Moreno-Simonet[7], Pedro L. Cosio[7], Joan A. Cadefau[7], Max Marwede[3] and Alfredo E. Ongaro[1]*

[1]Onalabs Inno-Hub SL, Barcelona, Spain, [2]Department of Mechanical Engineering, Universitat Politècnica de Catalunya-BarcelonaTech (UPC), Barcelona, Spain, [3]Environmental and Reliability Engineering Department, Fraunhofer IZM, Berlin, Germany, [4]Barcelona Institute for Global Health, ISGlobal, Barcelona, Spain, [5]Doctorate Program in Bioinformatics, Universitat Autònoma de Barcelona, Cerdanyola del Vallès, Spain, [6]Sigma Cognition, Madrid, Spain, [7]Institut Nacional d'Educació Física de Catalunya (INEFC), Barcelona, Spain

**Introduction:** Wearable sweat sensors are emerging as non-invasive tools for health monitoring and point-of-care diagnostics. However, their single-use nature and complex manufacturing processes pose significant sustainability challenges. This research integrates Life Cycle Assessment (LCA) at the design stage to address these environmental concerns, using it as a decision-making tool to guide material selection.

**Methods:** We developed an integrated capacitive sensor for continuous sweat rate and dehydration monitoring. The study's focus was on replacing conventional silver-printed electrodes with more sustainable alternatives. We specifically investigated the viability of using copper-based laminates and screen-printed graphite as alternative electrode materials, assessing their performance against the original silver electrodes. A comprehensive LCA was performed to evaluate the environmental footprint of the device's manufacturing and assembly processes.

**Results:** Our findings demonstrate that both copper-based laminates and screen-printed graphite are viable substitutes for silver-printed electrodes, maintaining functional performance while significantly reducing the device's environmental impact. The LCA data confirmed that these material substitutions lowered the overall environmental footprint of the wearable sweat sensors.

**Discussion:** This work underscores the critical role of integrating sustainability principles and tools like LCA early in the design phase of medical devices. By making informed material choices, it is possible to develop functional, high-performance wearable sensors that are also environmentally conscious. This approach offers a practical pathway toward scalable, sustainable, and net-zero healthcare technologies.

KEYWORDS

**life cycle assessment (LCA), wearables, sustainable medical devices, dehydration, sweat rate, sweat sensors**

## 1 Introduction

Wearable devices have emerged as transformative tools in healthcare and sports industries, enabling real-time physiological information for better insights of patients' wellbeing and athlete performance. These systems rely on data about step counts, GPS tracking and heart rate dynamics to calculate calorie expenditure, metabolic efficiency, sleep quality, stress markers, and ovulation phases (Babu et al., 2024). Such advancements represent a paradigm shift toward real-time, minimally invasive health tracking directly at the point of need (Chen et al., 2024).

The development of such tools, and the necessary infrastructure and knowledge to deploy and properly use them, marks a significant breakthrough from traditional invasive diagnostic methods, such as blood sampling, which are episodic, uncomfortable, and impractical for continuous monitoring outside clinical settings (Yang et al., 2024). Among these innovations, robust sweat analysis stands out as a promising non-invasive alternative to conventional biofluid sampling, enabling comprehensive detection platforms directly at the skin interface (Yang et al., 2024; Nelson et al., 2025).

The efficacy of wearable sweat sensors is underpinned by the combination of advanced microfluidic systems, to control the collection, transport, and real-time analysis of microliter range sweat samples; and miniaturized electronic platforms capable of multiplexed analyte detection and real-time data processing and transmission. Sweat is a gentle bio-fluid rich in biomarkers, including electrolytes, metabolites, and signaling molecules (i.e., sodium, ammonium, potassium, glucose, lactate, ketones, and cytokines) (Bandodkar et al., 2019; Gao et al., 2016; Kim et al., 2019). Its adoption as a biofluid holds broad implications across clinical diagnostics, athletic performance optimization, and preventive wellness management, potentially enabling earlier disease detection, individualized therapeutic interventions, and improved outcomes (Bandodkar and Wang, 2014; Xu et al., 2021).

Furthermore, sweat itself is a biomarker on its own right, providing insights about thermoregulation and hydration dynamics. In fact, the precise measurement of sweat rate is pivotal for assessing physiological parameters. It is essential for hydration monitoring in athletes and early diagnosis of conditions such as cystic fibrosis (Emaminejad et al., 2017). Recent works emphasize how wearable electrochemical systems are advancing remote hydration and health management by enabling continuous sweat-based assessments at the skin interface (Lee et al., 2025).

Capacitive sweat rate sensors, such as those developed by Choi et al. (2020), exemplify this approach: cost-effective, laser-cut microfluidic channels sandwiched between simple parallel conductive plates permit real-time, on-body tracking of sweat loss without complex fabrication steps (Baker et al., 2020; Ghaffari et al., 2021). These designs leverage changes in dielectric properties as sweat enters the channel to provide high-resolution sweat dynamics with minimal hardware. Collectively, innovations in microfluidic and capacitive embodiments are paving the way for accurate, wearable, continuous sweat rate sensing, completing the physiological picture delivered by sweat biomarker analysis and reinforcing the shift toward minimally invasive, real-time health tracking platforms.

Despite these benefits, the widespread adoption of single-use wearable devices introduces environmental challenges. Increased demand for electronics integration creates a tension between improved personal health tracking and rising electronic waste (e-waste) generation. Devices like continuous glucose monitors illustrate both the promise and environmental trade-offs of wearable health technologies. At present, most discarded devices, are treated as general medical or household waste, with limited recovery or recycling pathways. This means that valuable metals and plastics are lost, while electronic components often end up in landfills or incineration streams, illustrating the urgent need to balance technological promise with environmental responsibility. As Deman et al. ask "part of the problem or part of the solution?" (Cbr-Partner, 2025; Deman et al., 2024; Jo et al., 2021; Wöhrle et al., 2025), the future of point-of-care diagnostics must prioritize sustainability. Without conscious eco-design, these technologies risk exacerbating the global e-waste crisis, potentially negating their societal benefits (Ongaro et al., 2022). This highlights the urgent need to design the next-generation of wearable devices with environmental sustainability in mind, beginning with the integration of Life Cycle Assessment (LCA) at the earliest stages of design and development.

In our previous work, we presented a highly integrated sweat wearable system to perform real-time analysis of sweat loss, conductivity and lactate levels (Aguilar et al., 2020; Rabost-Garcia et al., 2023; Aguilar-Torán et al., 2023). This wearable system, now commercially available, consists of a durable part that integrates hardware electronic and communication systems, and a consumable device. Herein, we focus on the consumable device, a microfluidic cartridge that integrates skin adhesives, sweat management microfluidic channels, printed electronics for analyte sensing and a removable mechanical part for connection with the durable device. We demonstrate how LCA can be applied as a design tool to model and estimate the environmental impacts of the continuous sweat rate sensor for dehydration monitoring within the consumable microfluidic cartridge. Incorporating LCA during the development process enables early identification of environmental hot-spots and supports informed material and manufacturing decisions (Figure 1).

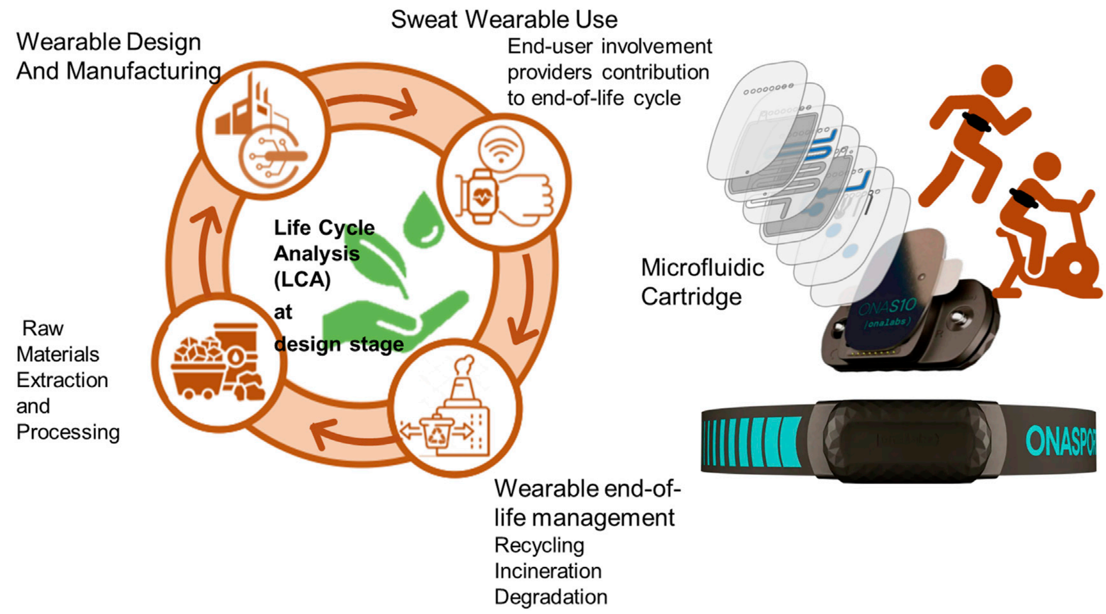


FIGURE 1
Life Cycle Assessment of a Sweat Wearable System with a Focus on the Microfluidic Cartridge. Left: Illustrative example of the life cycle of a sweat wearable system, from raw materials extraction to EoL management. Right: Illustration of the wearable system with a detailed view of the wearable device in use and exploded view of the microfluidic cartridge for sweat sample management and detection.

## 2 Materials and methods

### 2.1 Integrated capacitive sweat volume sensor in a microfluidic enclosure

Previous wearable sweat-rate technologies typically rely on microfluidic capture of sweat combined with optical or electrochemical readouts. For example, Gatorade's Gx sweat patch (Ghaffari et al., 2023) funnels sweat into a colorimetric microchannel and infers sweat rate, fluid loss and sodium loss from the channel filling pattern and dyes, while a recent study demonstrates a multimodal wearable that embeds electrochemical electrode arrays and biophysical sensors in microfluidic channels to continuously measure whole-body sweat loss (Spinelli et al., 2025). The presented sweat rate sensor design is based on a capacitive sensing mechanism integrated on a serpentine microfluidic structure. The device is attached to the skin of the wearer using a biocompatible adhesive, ensuring stable contact during physical activity. The sensor transduces sweat volume capacitively, as illustrated in Figure 2. When the wearer begins to sweat, sweat is actively pushed into the inlet by the natural sweating process and flows through the serpentine microchannel. As the sweat fills the channel, the two metal layers above and below the serpentine form a capacitor whose total capacitance increases (because ε_$H_2O$ ≫ ε_ air), enabling continuous monitoring of sweat accumulation. The serpentine design maximizes interaction between sweat and electrodes while keeping the sensor compact. The sweat then exits the channel through an outlet, allowing continuous flow and preventing overflow. By tracking capacitive changes along the serpentine path, the sensor calculates real-time sweat rate. Integrating this data over time, while accounting for physiological parameters, enables continuous dehydration prediction, providing insights into fluid loss during exercise or daily activity, without reliance on colorimetric reagents or optical readout.

### 2.2 Fabrication of the microfluidic cartridge with integrated capacitive sweat volume sensor

The microfluidic cartridge for sweat-rate monitoring was fabricated using laminate technology, which combines printed or laminated electrodes with laser-cut adhesive spacers (Figure 3). Screen-Printed Electrodes were fabricated on Autostat CT5 substrate with Silver (515 EI, Chimet) or graphite ink (Loctite EDAG PF 407 A, Henkel). Laminate electrodes were fabricated using Copper foil (3M 1181) converted to the desired shape with a die-cutter machine (Silhouette Cameo 2). A protective dielectric layer (ARcare 7815) was applied to prevent direct fluid contact with the electrode. The microfluidic channel is prepared by $CO_2$ laser-cutting (Epilog Fusion 30 W) a 230 µm-thick adhesive spacer (3M 7959) to form a serpentine channel. The layers were precisely aligned and laminated under controlled pressure, after which the vias were filled with conductive silver epoxy and the final device was diced via laser cutting to achieve individual sensor units. This method ensures rapid prototyping, design flexibility, and scalability for industrial production. A channel cross-section of 2 mm in width by 0.23 mm in height defined sweat enclosure in contact with hydrophilic surfaces with low wettability. At the bottom and top by a 2-mm-width channel surface of clear polyester film, the backing side or carrier of a single sided acrylic PSA (ARcare 7815) acting as dielectric layer of the electrode. The side walls of the microchannel (0.23 mm in height), are defined by the ablated double

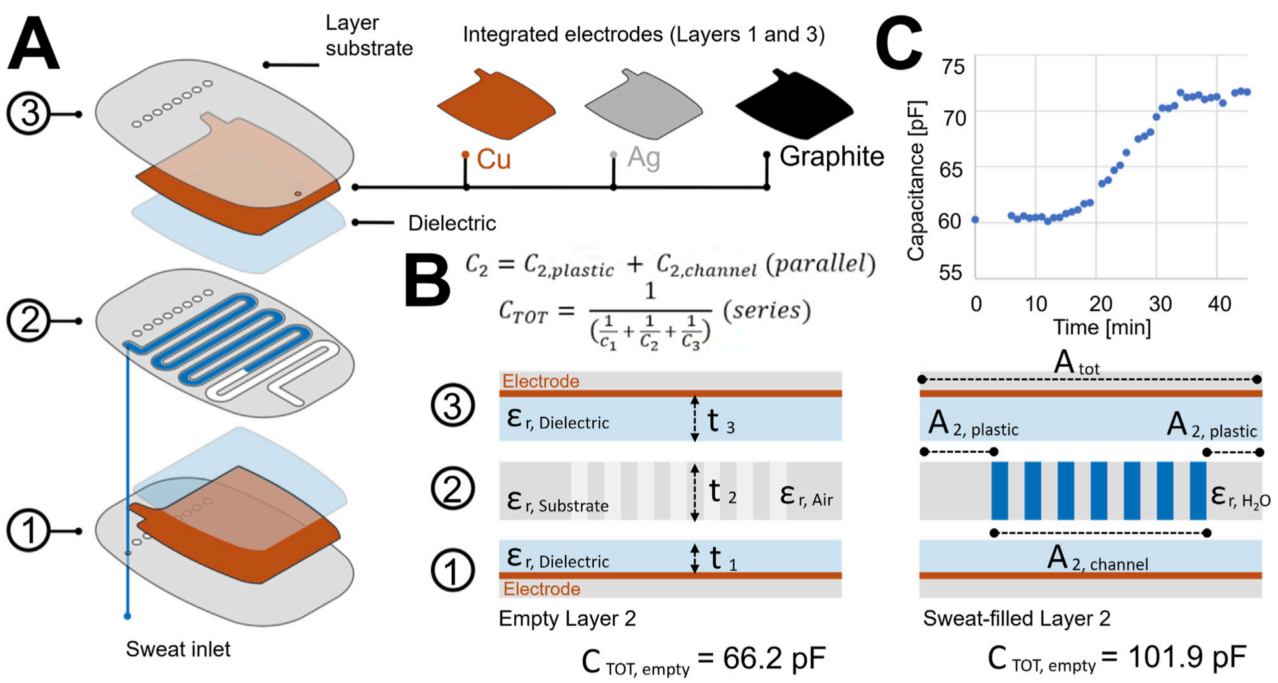


FIGURE 2
Integrated capacitive sweat volume sensor in a microfluidic enclosure: **(A)** Exploded schematic of the device layers. Layers 1 and 3 contain integrated metal electrodes (e.g., Cu, Ag, graphite) separated from the microfluidic channel layer (Chen et al., 2024) by dielectric films. The serpentine microfluidic channel (blue) in layer 2 receives sweat via an inlet and is sandwiched between the electrodes to form a parallel-plate capacitor. **(B)** Equivalent capacitance model. The total capacitance ($C_{tot}$) is determined by the series combination of capacitances from layers 1, 2, and 3. In layer 2, the capacitance arises from the plastic substrate ($C_{2,plastic}$) and the channel ($C_{2,channel}$) in parallel. The dielectric constant of water ($\varepsilon_r$,H2O) is significantly higher than that of air, so channel filling produces a measurable capacitance increase (empty: 66.2 pF; filled: 101.9 pF). **(C)** Representative capacitance measurement during sweat filling. Top: graph showing capacitance versus time, with a clear increase as the channel fills. Bottom: cross-sectional diagrams of the channel layer in empty (air-filled) and sweat-filled states, illustrating the increased effective dielectric constant ($A_{2,channel}$ region) during filling.

sided acrylic adhesive (50 microns) on a polyester film carrier 0.13 mm (3M 7959).

## 2.3 Life cycle analysis

LCA is a methodology that aims to model and estimate the environmental impacts of products and services throughout part of or the totality of its life cycle (International Organization for Standardization, 2006). Although LCA is usually employed for finished products and to quantify their environmental footprint, it can also be used as a design tool. By incorporating LCA into the design process, the environmental perspective can be implemented early on, helping to identify hot-spots and the best material or process alternatives. The flipside is that, since data is still scarce at the early stages of product developments, the accuracy of the LCA might result low. The main goal of this LCA is to assist the design process of the device to identify the environmental hot-spots early on, to allow for implementation of eco-design measures; and to quantify the improvement potential of said measures.

In this study, LCA was applied not only to quantify impacts but also to inform design choices. Specifically, it was used to compare electrode materials (silver, copper, graphite) and to identify manufacturing stages with the largest contribution to the overall footprint. These outputs guided the selection of material alternatives and highlighted opportunities to reduce impacts during production. The main goal of this LCA is therefore to support the design process by identifying environmental hot spots early on, enabling the implementation of eco-design measures, and quantifying the improvement potential of those measures.

In this paper, the focus will lie in the production phase of the device. This is for mainly two reasons: firstly, as it is common in low-energy electronic devices, the manufacturing phase is the main driver of most environmental impacts. Secondly, as this exercise focuses on giving the designers tools to improve their product, the production phase is the life cycle stage where the most direct control can be exerted. In order to provide a wider picture and detect possible trade-offs, this paper will evaluate several impact categories: Global Warming Potential (GWP), mineral resource use, water use and freshwater ecotoxicity, among others. The device analyzed is a consumable device that coupled with a durable device (ONASPORT) provides sweat metrics to the users. The microfluidic cartridge analyzed in this article can be schematized with two main parts: the sweat management and detection part, including the electronic functional components of the sensing electrodes.

The modelling of the device is based on a Bill of Materials (BoM) and contains data on the different parts, inks, substrates, and scrap materials that comprise the different parts of the microfluidic device. In the present analysis we considered three versions of the device

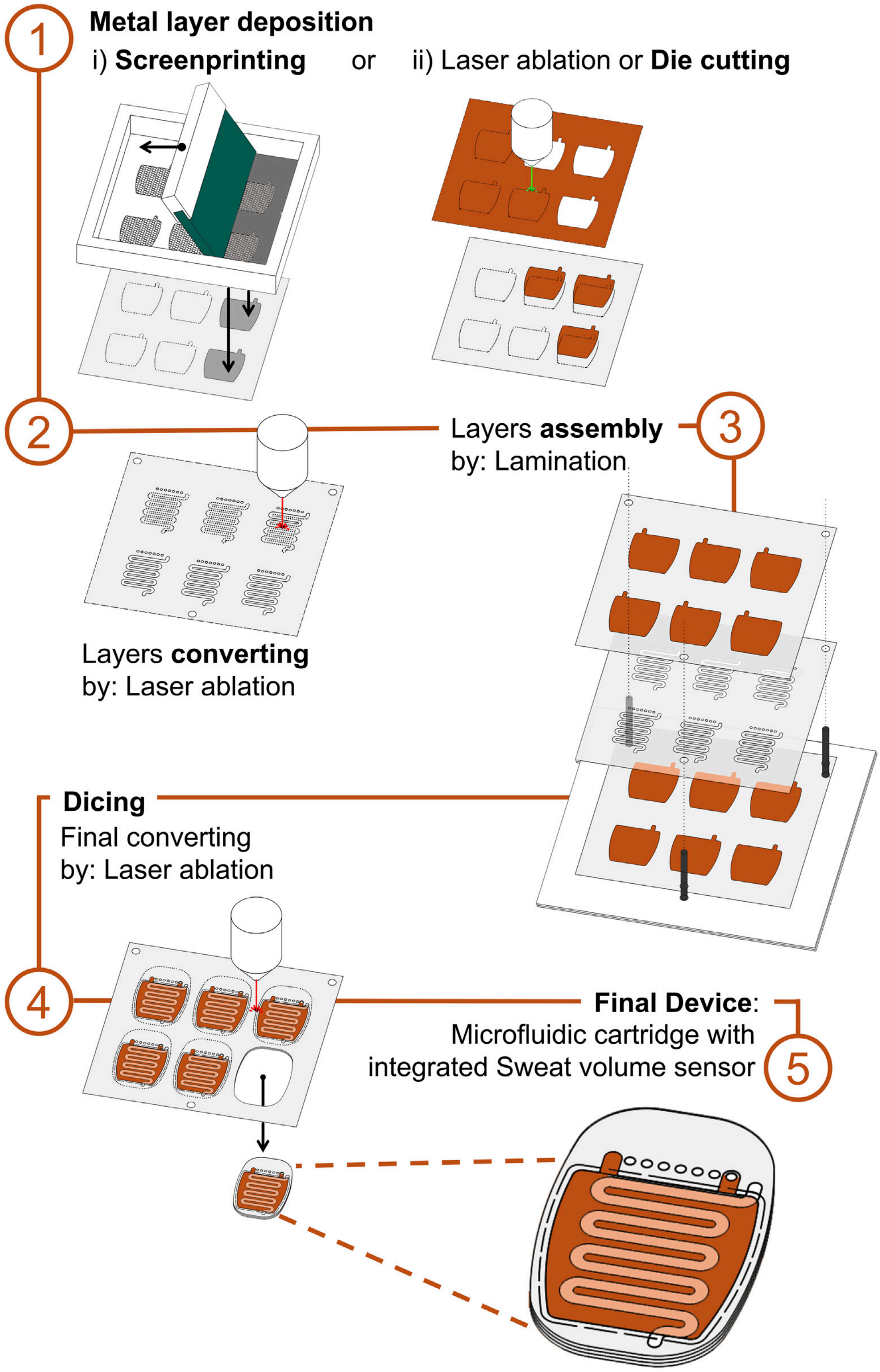


FIGURE 3
Schematic Representation of the device fabrication. 1) Sensing capacitive layer fabrication by i) screen printing (for Silver and Graphite) or ii) Die cutting (Copper foil); 2) Microstructuring of the serpentine microfluidic channel for sweat metering and volume analysis; 3) Layers assembly via an alignment and assembly tool; 4) Final device converting by laser-cutting of the individual sensor units; 5) Final microfluidic cartridge with integrated sweat volume sensor.

containing silver, copper or graphite electrodes. For the background data, both the Sphera Database v2025.1 (Sphera, 2025) and the Ecoinvent database v3.9.1 (Ecoinvent, 2025) have been used. For the modelling of the different inks a reworked version of the Ecoinvent dataset for the metallization paste (Ecoquery, 2025) has been used.

Whenever a suitable dataset couldn't be found, a proxy has been selected based on the material properties of the part or based on alternative materials used in the field. Wherever none could be found, the part or material was omitted in the analysis.

The model of the manufacturing process as such includes: the 3D printing of the nylon part for sweat management, the printing process of the electrodes and the laser cutting of the pieces. Energy consumption of 3D printing on nylon is based on literature data (Ulkir, 2023). In all cases the energy mix for the model is assumed to be the Spanish energy mix, as all these manufacturing activities take place there at the moment.

## 2.4 *In-vitro* characterization

To evaluate the performance of the different versions of the device, we employed a syringe pump (KDS-101-CE, KD Scientific) to compare capacitance changes across copper (cut/laminate), silver, and graphite electrodes. Capacitance measurements were recorded during microchannel filling with artificial sweat solution (EN1811: 2012/19), and key metrics, including sensitivity, linearity ($R^2$), and dynamic range, were compared across electrode types.

## 2.5 *In-vivo* characterization

Moving beyond benchtop validation, a proof-of-concept evaluation under real-world conditions of the sustainable copper-based sweat sensors was conducted during controlled 1-h cycling sessions for 25 participants. Total whole-body sweat loss and dehydration percentage (%) were estimated based on body weight difference before and after the training session using a mechanical scale with a stadiometer (PESPERSON S.L.). Careful consideration was dedicated to preventing sweat from being trapped in clothing, and drinking, eating or urination were not allowed to avoid affecting the water and mass balance (Cheuvront and Montain, 2017). The ONASPORT device (Onalabs Inno-Hub) was worn throughout the 1-h training session, monitoring the sweat volume collected by the microfluidic cartridge. Sweat loss was calculated using an adapted regional to whole-body conversion model (Baker et al., 2018). Sweat loss was validated comparing the output value from the ONASPORT at the end of the training session with the body weight difference.

The data from 25 exercise sessions involving male and female participants (body mass: 54.5–93.5 kg) with complete pre- and post-exercise body weight measurements and corresponding sweat loss estimates were analyzed as follows. For each session, dehydration was calculated as: 1) "Reference dehydration" = (Weight_before − Weight_after)/Weight_before; 2) "Estimated dehydration" = Sweat_loss/Weight_before); and "Prediction error" = Estimated dehydration − Reference dehydration.

The prediction error served as the dependent variable for model development. Data were split into training (n = 15) and test (n = 10) sets using stratified sampling to balance sex distribution and weight range. A simple linear regression model was fitted on the training set to predict systematic error as a function of body mass. Predicted error corrections were subtracted from original sweat loss estimates to produce corrected dehydration values. Model performance on the test set was assessed using mean absolute error (MAE), root mean square error (RMSE), bias, and Pearson correlation. Agreement between reference and corrected methods was evaluated using Bland–Altman analysis, and the Wilcoxon signed-rank test was applied to compare absolute errors before and after correction.

# 3 Results and discussions

## 3.1 LCA analysis tool

The LCA focused on the production phase of the device, including fabrication and assembly of all functional components, i.e., sweat management and printed electronics. The key finding was that printed electronic components, (silver screen-printed electrodes, copper laminate, and graphite screen-printed electrodes) dominated the environmental impacts, contributing for approximately 60%–90% across the assessed categories (Figure 4). The estimated GWP for the silver-design based was 0.149 kg $CO_2$e, with silver inks responsible for the majority of this burden due to the energy-intensive mining and ink formulation processes. Substitution with copper laminate yielded the largest reduction in GWP, followed by graphite ink, with both alternatives also reducing mineral resource use, water use, and freshwater ecotoxicity.

Breaking down the printed components into substrates, inks, and printing processes (Figure 4) revealed that ink selection was the primary driver of environmental performance. Silver ink showed both the highest embodied material impact and the greatest printing energy requirement, largely due to long curing times. Copper laminate had intermediate embodied material impacts but the lowest printing energy demand, as no curing was required. Graphite ink displayed the lowest embodied impact, though its curing requirements resulted in intermediate printing energy use. In all non-GWP categories (Figure 4), the performance ranking was consistent: silver had the highest impact, with copper and graphite showing similar improvements. These findings highlight that targeting the functional printed elements, especially ink choice, is the most effective route to improve sustainability and to achieve significant environmental benefits. This is complementary to previous sustainability studies on microfluidic and point-of-care devices, which commonly focus specifically on the bulk microfluidic materials.

This LCA was performed during the development of the different prototypes, which means that not all the data ideally needed for an accurate assessment was available. Thus, the main limitations of the current model are as follows. The formulation of the different inks is largely unknown and therefore is assumed to be the same for all, just replacing the core conductive material. While this seems fair in that ultimately this material seems to drive the environmental impacts of the ink, it does not reflect potential differences in the different ink formulations that may have an impact on their environmental performance. Besides, the printing process is modelled using a mix of primary and secondary data and

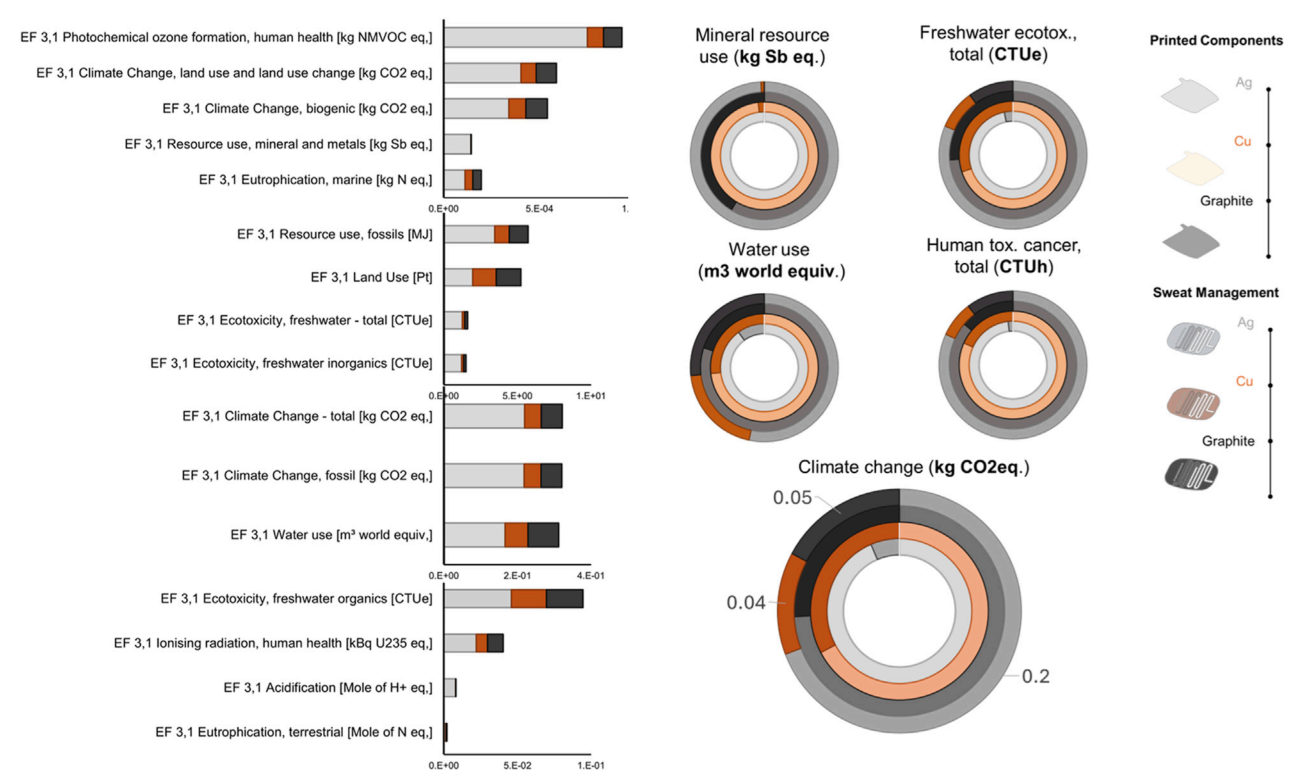


FIGURE 4
Environmental Impact Assessment of Printed Components and Sweat Management Materials. Bar plots represent the quantified environmental impacts of each material in several impact categories. Key indicators include: Climate change (kg $CO_2$ eq.); Resource use (mineral and fossil); Water use ($m^3$ world equiv.); Freshwater ecotoxicity (CTUe); Human toxicity (cancer and non-cancer effects); Eutrophication and acidification; Ionising radiation; Photochemical ozone formation, and more. Bar is color-coded according to the material: (Light gray Silver (Ag); Orange Copper (Cu); Dark gray Graphite). Right Panel: Donut charts highlight five key impact categories in more detail: Mineral resource use (kg Sb eq.); Freshwater ecotoxicity, total (CTUe); Water use ($m^3$ world equiv.); Human toxicity, cancer effects (CTUh); Climate change (kg $CO_2$ eq.). For each donut plot: The three inner rings correspond to the comparison of the Printed Components (clearer colors) with the Sweat Management components (darker color) for each material (silver, copper and graphite, from inner to outer). The last outer ring is a comparison of the total impact (printed plus sweat management) of the three different materials.

given the pivotal role it plays in the results, it still needs to be refined in order to make the conclusions more sound. Finally, the model presented here covers only the production phase. However, the material selection may have effects further down the life cycle, especially in the End-of-Life (EoL) of the product, that also warrant consideration. For example, the electrodes are not reusable and thus such considerations are relevant for the material choice.

## 3.2 *In-vitro* test: characterization of the sweat rate sensor

Capacitive sweat sensors with silver, copper, and graphite electrodes were characterized *in-vitro* (Figure 5). All devices exhibited a stable basal period in the air-filled state, followed by a near-linear increase with injected volume up to saturation. Laminated copper electrodes demonstrated the highest sensitivity, though their calibration curve showed a slight quadratic non-linearity ($R^2$ = 0.98). The other two configurations exhibited nearly perfect linearity ($R^2 \approx 0.998$) with slightly lower sensitivities. Importantly, the improved sensitivity of laminated copper did not reduce the usable linear range, indicating that manufacturing adjustments could improve performance without sacrificing sensor dynamics. However, when assessed using average relative deviation from reference volumes between sensor replicas, silver electrodes significantly outperform the alternatives, with a mean deviation of approximately 7.5% compared to 20.3% for graphite and 20.9% for copper. These results indicate that while copper and graphite substantially improve sustainability, further optimization of their fabrication or calibration may be required to match the prediction accuracy of silver electrodes.

To provide a holistic performance assessment (Figure 5D), additional Key Performance Indicators (KPIs) were analyzed based on material properties and manufacturing considerations. Cost and Ease of Fabrication were pivotal economic factors; the high price of silver as a precious metal contrasts sharply with the low cost of copper and graphite (Li et al., 2021). The fabrication process for all materials was well-established, with silver and graphite inks leveraging mature printing techniques and copper foil utilizing precise die-cutting. Durability was evaluated based on the stability and resistance of the materials to environmental degradation in literature (Li et al., 2021). The Linear Range of both metal electrodes was deemed wide and stable due to the inherent properties of the materials, while the range for graphite was considered more moderate due to potential variability in its

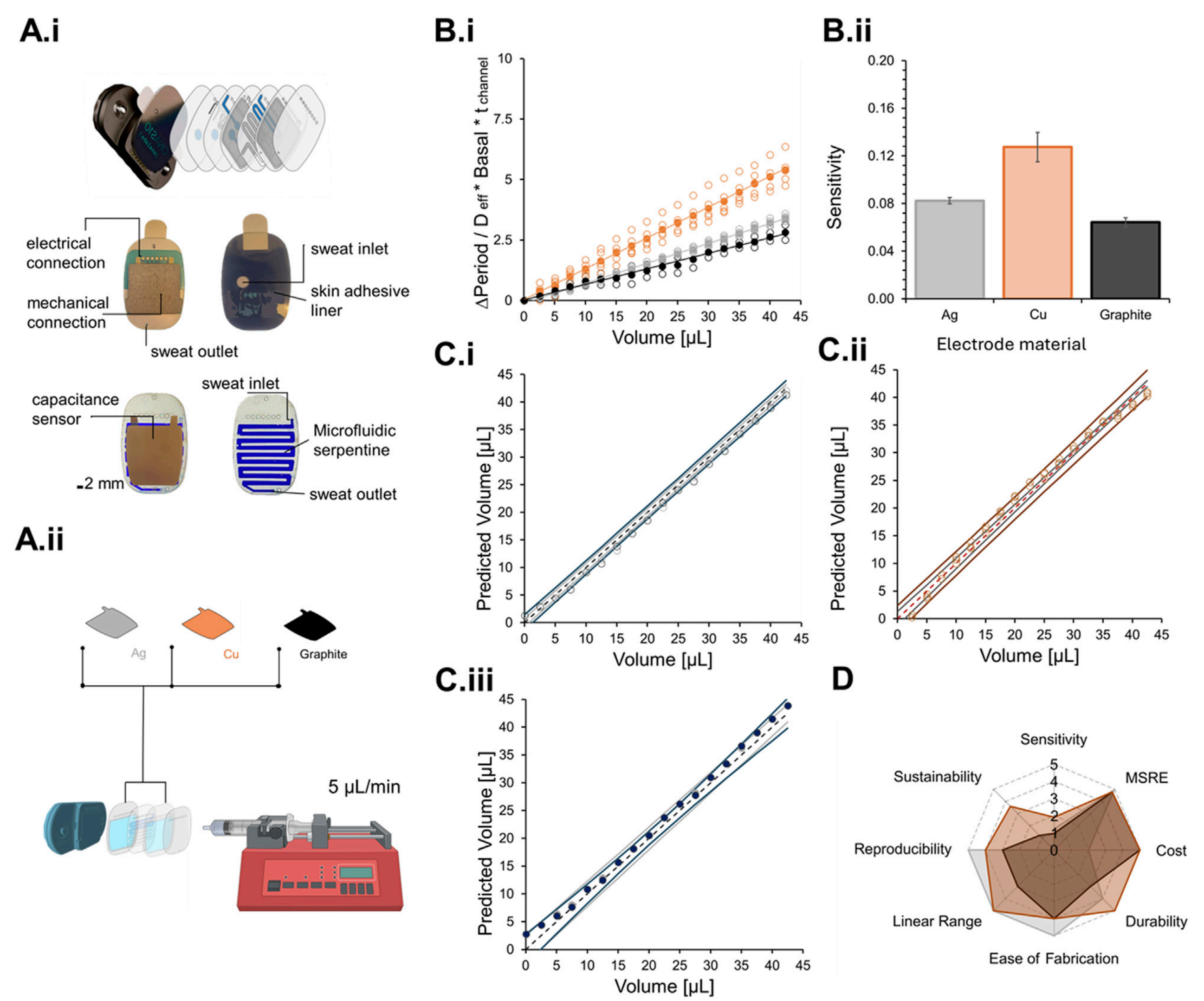


FIGURE 5
Performance Evaluation of Printed Electrode Materials for Sweat Volume Sensing. **(Ai)** Picture of the ONASPORT device with schematic of the microfluidic cartridge. Below, pictures of the microfluidic cartridge (exterior part for the connection with ONASPORT, top left, and interaction with the wearer, top right, and pictures of the layers related to the sweat volume sensor, bottom left and right). The picture showcasing the serpentine, bottom right, is filled with methylene blue. **(Aii)** Schematic representation of the experimental setup used to evaluate sweat sensor performance. Electrodes made from three printed materials—Silver (Ag, light gray), Copper (Cu, orange), and Graphite (black) are integrated into sweat sensors. A syringe pump delivers fluid at a constant flow rate of 5 µL/min for controlled volume testing. **(Bi)** Plot showing the normalized signal response (ΔPeriod/D_eff × Basal × L_channel) as a function of delivered volume for each electrode material. Data points represent mean values with standard deviation; open circles indicate increasing signal with volume for Ag (gray), Cu (orange), and Graphite (black). **(Bii)** Bar graph comparing the sensitivity of each electrode material. Copper shows the highest sensitivity, followed by silver and graphite. Error bars denote standard deviation. **(Ci–Ciii)** Linear regression plots comparing predicted vs. actual delivered volumes for: Silver electrodes (gray), Copper electrodes (orange), and Graphite electrodes (black), respectively. **(D)** Radar chart benchmarking the three electrode materials across eight performance metrics: Sensitivity; MSRE; Cost; Durability; Ease of Fabrication; Linear Range; Reproducibility and Sustainability.

carbon-based structure. Reproducibility was a key quality control metric; silver and copper foil electrodes showed superior consistency due to the uniformity of their source materials and processes, whereas graphite faced challenges with batch-to-batch variation (Suresh et al., 2021). Finally, sustainability was also considered, reflecting the broader environmental impact of material sourcing and disposal (Wiklund et al., 2021). Ultimately, this comprehensive evaluation revealed that while laminated copper offered superior sensitivity, it demonstrated the highest MSRE, indicating a trade-off in precision. Conversely, screen-printed silver achieved the lowest MSRE, but at a significantly higher cost, highlighting the crucial balance between performance, practicality, and cost in the final material selection. These findings underscore the importance of balancing accuracy, practicality, and sustainability when selecting electrode materials.

## 3.3 *In-vivo* test: continuous sweat rate and dehydration prediction

Laminated copper electrodes were evaluated *in-vivo* during controlled exercise (Figure 6). Sweat rate traces showed the

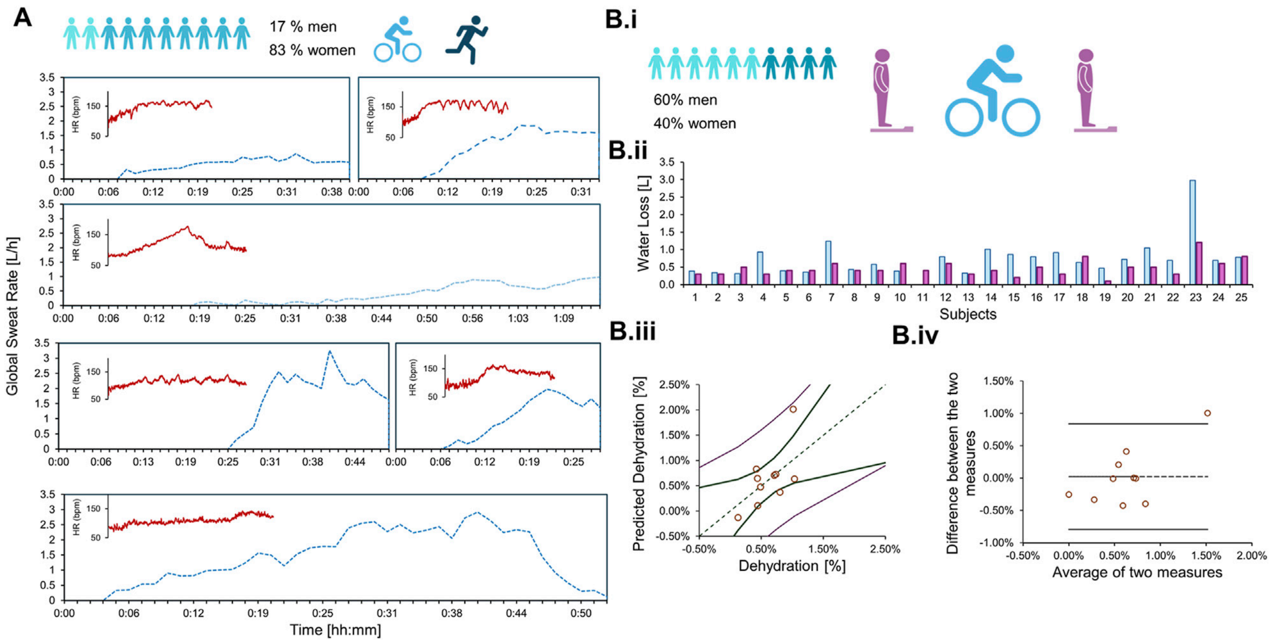


FIGURE 6
*In-vivo* proof of concept: field performance and physiological relevance. **(A)** Protocol summary (on top) and in-vivosweat rate graphs (on the bottom). In insert, the heart rate in bpm of the volunteers during the test. **(B)** Predicted versus Measured dehydration. (B.i): Population demographics of the 25 volunteers, of which 60% men and 40% women. The sport activity performed was cycling. (B.ii): Bar graph showing the total water loss (L) for each subject, with purple bars representing the water loss measured by the weight difference and the light blue bars the water loss measured by the proposed sensor. (B.iii): Linear regression of the predicted dehydration versus the measured dehydration. Purple line represents the prediction interval and the black line represents the 95% confidence interval. Red circles indicate individual data points. (B.iv): iBland-Altman plot. The dashed line indicates the mean difference and the continuous line the 95% limits of agreement. The red circles are individual data points.

expected rise during activity onset, plateau during steady exertion, and a delayed decline during recovery relative to heart rate, which is added in the plot to reflect activity level, consistent with the typical persistence of sweating after exercise stops (Figure 6A). Device-derived dehydration estimates, calculated from integrated sweat loss (Figure 6Bii), were consistent with those obtained from pre/post body mass measurements. The linear correction model reduced systematic error, yielding improvements in both MAE and RMSE in the test set. Pearson correlation between sensor-derived and reference dehydration increased post-correction (from 0.36 to 0.90), and Bland–Altman analysis indicated narrower limits of agreement (Figure 6B iii,iv).

For dehydration estimation, the mean squared relative error (MSRE) was 0.70, corresponding to an average relative deviation of approximately 84%. However, given the small magnitude of dehydration values, the MAE was only 0.31 percentage points, which is within the range reported for other wearable hydration monitors (e.g., normalized root-mean-square error ≈2%) (Rodin et al., 2022; Sabry et al., 2022) These results confirm that copper electrodes are suitable for continuous physiological monitoring, and that calibration adjustments can improve predictive accuracy.

Overall, combining LCA, *in-vitro*, and *in-vivo* findings shows that sustainable electrodes like copper and graphite can enable environmentally friendly sweat sensors without substantially compromising performance, provided fabrication and calibration are optimized. This has important implications for the development of next-generation wearable hydration monitors, highlighting the need to balance environmental impact, cost, and accuracy.

## 3.4 Limitations and outlook

While the integration of LCA into the design phase provided valuable insights for material substitution and manufacturing process optimization, it addresses only one aspect of sustainable product development. LCA is most effective when embedded within a broader circular design strategy that also considers business models, user behavior, and EoL management. The current study focused on the production stage; however, the choice of electrode material and integration method may influence downstream processes such as disassembly, material recovery, and recyclability. To fully realize the sustainability potential of wearable diagnostics, these factors must be addressed alongside environmental footprint reduction during manufacturing.

Circular business models: for example, take-back schemes, refurbishment loops, or component reuse, can extend product value beyond single use and reduce overall material demand. For disposable health-monitoring platforms, a “component harvesting” approach in which functional layers such as electrodes are reclaimed and reprocessed could complement the environmental gains identified in the present LCA.

Sector-wide initiatives such as the White Dot initiative (Indeed-Innovation, 2025) which connects manufacturers, recyclers, and regulators to create closed-loop supply chains for medical devices, illustrate how sector-wide collaboration can standardize material choices, improve design-for-disassembly guidelines, and coordinate post-use collection and processing. Beyond material and manufacturing considerations, digital functionalities such as AI-based analytics introduce their own sustainability challenges. For example, AI-enabled personalization in wearable diagnostics requires large, high-quality datasets, yet collecting such data, especially for emerging biomarkers like dehydration, can be resource-intensive, time-consuming, and environmentally burdensome.

One alternative approach is the use of generative AI to create synthetic datasets that replicate the statistical characteristics of real-world measurements without containing personal or sensitive information. This method reduces the need for extensive physical data collection, thereby lowering material use, energy consumption, and carbon emissions associated with large-scale trials. Furthermore, adopting energy-efficient AI algorithms and low-power processing architectures can minimize the computational footprint of onboard analytics. In this way, sustainability principles can be embedded not only in the physical design and production of wearable devices but also in their digital intelligence, ensuring that both hardware and software contribute to reduce environmental impact across the product lifecycle.

# 4 Conclusion

This study demonstrates the influential role of LCA as an impactful design tool at early stages of the development of wearable microfluidic sensors. By focusing on the functional transduction layer, we identified printed electrodes as the dominant contributor to production-phase environmental impacts. Replacing silver screen-printed electrodes with graphite alternatives or copper laminates significantly reduced GWP, mineral resource use, water consumption, and freshwater ecotoxicity. From a performance standpoint, laminated copper electrodes achieved the highest *in-vitro* sensitivity, while silver electrodes provided superior reproducibility. Graphite electrodes offered the lowest embodied environmental impact but required further optimization to reduce variability. Importantly, *in-vivo* testing of the copper-based devices confirmed their ability to track sweat dynamics and provide dehydration estimates consistent with reference body-mass measurements.

Taken together, these findings highlight a key trade-off between environmental sustainability and diagnostic performance: copper provides a favorable balance, delivering both substantial environmental gains and robust sensing performance with only minor calibration adjustments.

Overall, this work provides a replicable framework for integrating sustainability into the design of microfluidic and point-of-care devices. Embedding LCA in the earliest stages of product development, and coupling it with circular design principles, can help accelerate the transition towards net-zero healthcare technologies.

# Data availability statement

The original contributions presented in the study are included in the article/supplementary material, further inquiries can be directed to the corresponding author.

# Ethics statement

The studies involving humans were approved by the Ethics Committee for Clinical Research of the Catalan Sports Council (Generalitat de Catalunya) (037/CEICGC/2021). The studies were conducted in accordance with the local legislation and institutional requirements. The participants provided their written informed consent to participate in this study.

# Author contributions

GR-G: Conceptualization, Formal Analysis, Investigation, Methodology, Validation, Writing – original draft, Writing – review and editing. DS: Writing – original draft, Data curation, Formal Analysis, Investigation, Methodology, Visualization. VN-C: Formal Analysis, Investigation, Validation, Writing – original draft. AF: Formal Analysis, Investigation, Methodology, Validation, Writing – original draft. OY: Data curation, Investigation, Methodology, Visualization, Writing – original draft, Writing – review and editing. XM-P: Funding acquisition, Resources, Writing – review and editing. AA: Investigation, Software, Supervision, Writing – review and editing. JP-V: Conceptualization, Methodology, Resources, Supervision, Writing – review and editing. JC-T: Resources, Writing – review and editing. RH: Formal Analysis, Writing – original draft, Writing – review and editing. FE: Formal Analysis, Writing – review and editing. LM-S: Validation, Writing – review and editing. PC: Validation, Writing – review and editing. JC: Writing – review and editing, Investigation, Validation. MM: Resources, Writing – review and editing, Funding acquisition. AO: Conceptualization, Formal Analysis, Project administration, Resources, Supervision, Visualization, Writing – original draft, Writing – review and editing.

# Funding

The author(s) declare that financial support was received for the research and/or publication of this article. Part of this work was carried out as part of SUSTRONICS project that is co-funded by the European Union under grant agreement 101112109. Views and opinions expressed are however those of the authors only and do not necessarily reflect those of the European union or Chips Joint Undertaking. Neither the European Union nor the granting authority can be held responsible for them. This project is supported by the Chips Joint Undertaking and its members under grant agreement 101112109 including top up funding by Netherlands, Austria, Germany, Spain, Finland, France, Latvia, Poland and Sweden. This work also received funding from the Swiss State Secretariat for Education, Research and Innovation (SERI).

# Acknowledgments

VN acknowledges the Generalitat de Catalunya, with the support of the Agència de Gestió d’Ajuts Universitaris i de Recerca (AGAUR), the Consorci de Serveis Universitaris de

Catalunya (CSUC), and the collaboration of the Fundació Catalana per a la Recerca i la Innovació (FCRI), with reference 2024 DI 00102 and through the CERCA Program and the grant CEX2023-0001290-S funded by MCIN/AEI/10.13039/501100011033. GR acknowledges the Agència de Gestió d'Ajuts Universitaris i de Recerca (AGAUR) from Generalitat de Catalunya for the Industrial PhD grant with reference 2019 DI 18.

## Conflict of interest

Authors GR-G, VN-C, AF, OY, XM-P, AA, JP-V, and AO were employed by Onalabs Inno-Hub SL.

Authors RH, and FE were employed by Sigma Cognition.

The remaining authors declare that the research was conducted in the absence of any commercial or financial relationships that could be construed as a potential conflict of interest.

## Generative AI statement

The author(s) declare that Generative AI was used in the creation of this manuscript. The authors used generative AI tool (e.g., ChatGPT, Gemini) as a productivity and editing assistant for minor tasks, including checking for spelling and grammar, style consistency, and improving sentence clarity. The AI tool did not perform any core tasks such as data analysis, interpretation, or the generation of original content or arguments. All intellectual contributions and creative works are the sole responsibility of the authors.

Any alternative text (alt text) provided alongside figures in this article has been generated by Frontiers with the support of artificial intelligence and reasonable efforts have been made to ensure accuracy, including review by the authors wherever possible. If you identify any issues, please contact us.

## Publisher's note



## References

Aguilar, J., Alvarez-Carulla, A., Colmena, V., Carreras, O., Rabost, G., Puig-Vidal, M., et al. (2020). "Autonomous self-powered potentiostat architecture for biomedical wearable applications," in 2020 35th Conference on Design of Circuits and Integrated Systems, DCIS 2020, Segovia, Spain, 18-20 November 2020 (IEEE).

Aguilar-Torán, J., Rabost-Garcia, G., Toinga-Villafuerte, S., Álvarez-Carulla, A., Colmena-Rubil, V., Fajardo-Garcia, A., et al. (2023). Novel sweat-based wearable device for advanced monitoring of athletic physiological biometrics. *Sensors* 23 (23), 9473. doi:10.3390/s23239473

Babu, M., Lautman, Z., Lin, X., Sobota, M. H. B., and Snyder, M. P. (2024). Wearable devices: implications for precision medicine and the future of health care. *Annu. Rev. Med.* 75, 401–415. doi:10.1146/annurev-med-052422-020437

Baker, L. B., Ungaro, C. T., Sopeña, B. C., Nuccio, R. P., Reimel, A. J., Carter, J. M., et al. (2018). Body map of regional vs. whole body sweating rate and sweat electrolyte concentrations in men and women during moderate exercise-heat stress. *J. Appl. Physiol.* 124 (5), 1304–1318. doi:10.1152/japplphysiol.00867.2017

Baker, L. B., Model, J. B., Barnes, K. A., Anderson, M. L., Lee, S. P., Lee, K. A., et al. (2020). Skin-interfaced microfluidic system with personalized sweating rate and sweat chloride analytics for sports science applications. *Sci. Adv.* 6 (50), 3929–3940. doi:10.1126/sciadv.abe3929

Bandodkar, A. J., and Wang, J. (2014). Non-invasive wearable electrochemical sensors: a review. *Trends Biotechnol.* 32 (7), 363–371. doi:10.1016/j.tibtech.2014.04.005

Bandodkar, A. J., Gutruf, P., Choi, J., Lee, K. H., Sekine, Y., Reeder, J. T., et al. (2019). Battery-free, skin-interfaced microfluidic/electronic systems for simultaneous electrochemical, colorimetric, and volumetric analysis of sweat. *Sci. Adv.* 5 (1), eaav3294. doi:10.1126/sciadv.aav3294

Cbr-Partner (2025). Life cycle assessment (LCA) in MedTech. Available online at: https://cbr-partner.de/article/life-cycle-assessment-lca-in-medtech/.

Chen, X., Kim, D. H., and Lu, N. (2024). Introduction: wearable devices. *Chem. Rev.* 124 (10), 6145–6147. doi:10.1021/acs.chemrev.4c00271

Cheuvront, S. N., and Montain, S. J. (2017). Myths and methodologies: making sense of exercise mass and water balance. *Exp. Physiol.* 102 (9), 1047–1053. doi:10.1113/ep086284

Choi, D. H., Gonzales, M., Kitchen, G. B., Phan, D. T., and Searson, P. C. (2020). A capacitive sweat rate sensor for continuous and real-time monitoring of sweat loss. *ACS Sens.* 5 (12), 3821–3826. doi:10.1021/acssensors.0c01219

Deman, A. L., Guijt, R. M., Odhiambo, C. O., Ndlovu, Z., and Kersaudy-Kerhoas, M. (2024). Part of the problem or part of the solution? An interdisciplinary action call for more research on the environmental sustainability of lab-on-a-chip and point-of-care devices. *Front. Lab a Chip Technol.* 3, 1530449. doi:10.3389/frlct.2024.1530449

Ecoquery (2025). Metallization paste production, front side - europe - metallization paste. Available online at: https://ecoquery.ecoinvent.org/3.11/cutoff/dataset/2180/documentation.

Emaminejad, S., Gao, W., Wu, E., Davies, Z. A., Yin Yin Nyein, H., Challa, S., et al. (2017). Autonomous sweat extraction and analysis applied to cystic fibrosis and glucose monitoring using a fully integrated wearable platform. *Proc. Natl. Acad. Sci. U. S. A.* 114 (18), 4625–4630. doi:10.1073/pnas.1701740114

Gao, W., Emaminejad, S., Nyein, H. Y. Y., Challa, S., Chen, K., Peck, A., et al. (2016). Fully integrated wearable sensor arrays for multiplexed *in situ* perspiration analysis. *Nature* 529 (7587), 509–514. doi:10.1038/nature16521

Ghaffari, R., Yang, D. S., Kim, J., Mansour, A., Wright, J. A., Model, J. B., et al. (2021). State of sweat: emerging wearable systems for real-time, noninvasive sweat sensing and analytics. *ACS Sens.* 6 (8), 2787–2801. doi:10.1021/acssensors.1c01133

Ghaffari, R., Aranyosi, A. J., Lee, S. P., Model, J. B., and Baker, L. B. (2023). The Gx sweat patch for personalized hydration management. *Nat. Rev. Bioeng.* 1 (1), 5–7. doi:10.1038/s44222-022-00005-5

Indeed-Innovation (2025). How MedTech can profit from circular economy. Available online at: https://www.indeed-innovation.com/the-mensch/the-white-dot-feasibility-study-shows-how-medtech-can-profit-from-circular-economy/.

Jo, S., Sung, D., Kim, S., and Koo, J. (2021). A review of wearable biosensors for sweat analysis. *Biomed. Eng. Lett.* 11 (2), 117–129. doi:10.1007/s13534-021-00191-y

Kim, J., Campbell, A. S., de Ávila, B. E. F., and Wang, J. (2019). Wearable biosensors for healthcare monitoring. *Nat. Biotechnol.* 37 (4), 389–406. doi:10.1038/s41587-019-0045-y

Lee, S. P., Aranyosi, A. J., and Ghaffari, R. (2025). Wearable electrochemical biosensors for remote hydration and health management. *Nat. Rev. Electr. Eng.* 2 (6), 371–372. doi:10.1038/s44287-025-00184-4

Li, Z., Chang, S., Khuje, S., and Ren, S. (2021). Recent advancement of emerging nano copper-based printable flexible hybrid electronics. *ACS Nano* 15 (4), 6211–6232. doi:10.1021/acsnano.1c02209

Nelson, R. S., Grossman, M. G., Klug, Z. M., Calamari, M., Donayre, A., Cybulski, T., et al. (2025). Remote analysis and management of sweat biomarkers using a wearable microfluidic sticker in adult cystic fibrosis patients. *Proc. Natl. Acad. Sci. U. S. A.* 122 (33), e2506137122. doi:10.1073/pnas.2506137122

Ongaro, A. E., Ndlovu, Z., Sollier, E., Otieno, C., Ondoa, P., Street, A., et al. (2022). Engineering a sustainable future for point-of-care diagnostics and single-use microfluidic devices. *Lab. Chip* 22 (17), 3122–3137. doi:10.1039/d2lc00380e

Rabost-Garcia, G., Colmena, V., Aguilar-Torán, J., Vieyra Galí, J., Punter-Villagrasa, J., Casals-Terré, J., et al. (2023). Non-invasive multiparametric approach to determine sweat-blood lactate bioequivalence. *ACS Sens.* 8 (4), 1536–1541. doi:10.1021/acssensors.2c02614

Rodin, D., Shapiro, Y., Pinhasov, A., Kreinin, A., and Kirby, M. (2022). An accurate wearable hydration sensor: real-World evaluation of practical use. *PLoS One* 17 (8), e0272646. doi:10.1371/journal.pone.0272646

Sabry, F., Eltaras, T., Labda, W., Hamza, F., Alzoubi, K., and Malluhi, Q. (2022). Towards On-Device dehydration monitoring using machine learning from wearable device's data. *Sensors (Basel)* 22 (5), 1887. doi:10.3390/s22051887

Spinelli, J. C., Suleski, B. J., Wright, D. E., Grow, J. L., Fagans, G. R., Buckley, M. J., et al. (2025). Wearable microfluidic biosensors with haptic feedback for continuous monitoring of hydration biomarkers in workers. *NPJ Digit. Med.* 8 (1), 76–12. doi:10.1038/s41746-025-01466-9

Suresh, R. R., Lakshmanakumar, M., Arockia Jayalatha, J. B. B., Rajan, K. S., Sethuraman, S., Krishnan, U. M., et al. (2021). Fabrication of screen-printed electrodes: opportunities and challenges. *J. Mater. Sci.* 56 (15), 8951–9006. doi:10.1007/s10853-020-05499-1

Wiklund, J., Karakoç, A., Palko, T., Yiğitler, H., Ruttik, K., Jäntti, R., et al. (2021). A review on printed electronics: fabrication methods, inks, substrates, applications and environmental impacts. *J. Manuf. Mater. Process.* 5 (3) 89. ;doi:10.3390/jmmp5030089

Wöhrle, M. L., Street, A., and Kersaudy-Kerhoas, M. (2025). Mass of components and material distribution in lateral flow assay kits. *Bull. World Health Organ* 103 (4), 236–246. doi:10.2471/blt.24.292167

Xu, J., Fang, Y., and Chen, J. (2021). "Wearable biosensors for non-invasive sweat diagnostics."*Biosensors* 11. MDPI, 245. doi:10.3390/bios11080245

Yang, G., Hong, J., and Park, S. B. (2024). Wearable device for continuous sweat lactate monitoring in sports: a narrative review. *Front. Physiol.* 15, 1376801. doi:10.3389/fphys.2024.1376801